

SUPPORTING INFORMATION

Potential of High Thermoelectric Efficiency of Silver Selenide

*Tristan Day,¹ Fivos Drymiotis,¹ Tiansong Zhang,² Daniel Rhodes,³ Xun Shi,²
Lidong Chen,² G. Jeffrey Snyder^{1,*}*

¹Department of Materials Science, California Institute of Technology, 1200 E. California Blvd, Pasadena, CA, 91104 (U.S.A.)

²CAS Key Laboratory of Energy-conversion Materials, Shanghai Institute of Ceramics, Chinese Academy of Sciences, Shanghai, 200050, (China)

³National High Magnetic Field Laboratory, Florida State University, Tallahassee, Florida, 32310, (U.S.A.)

e-mail: jsnyder@caltech.edu

1 Heat Capacity

The onset of the superionic transition is approximately 407 K, (Figures S1 and S2, insets show proximity to Dulong-Petit heat capacity) and the maximum in C_p occurs at 415 K. The enthalpy change of the phase transition is 25.3 kJ kg⁻¹, with a standard deviation of 0.2 kJ kg⁻¹. Dividing the enthalpy change by the phase transition temperature yields the entropy change of the phase transition, 0.062 kJ kg⁻¹ K⁻¹.

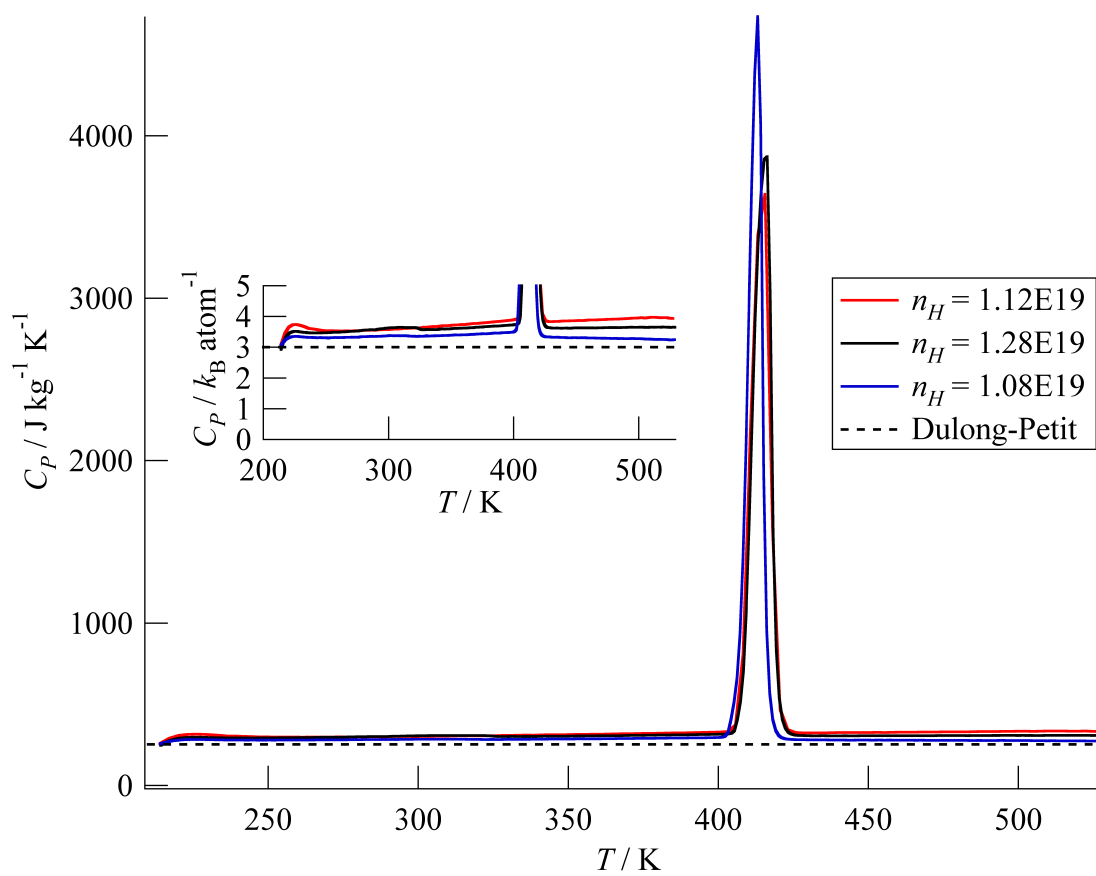


Figure S1: Heat capacity of hot-pressed samples

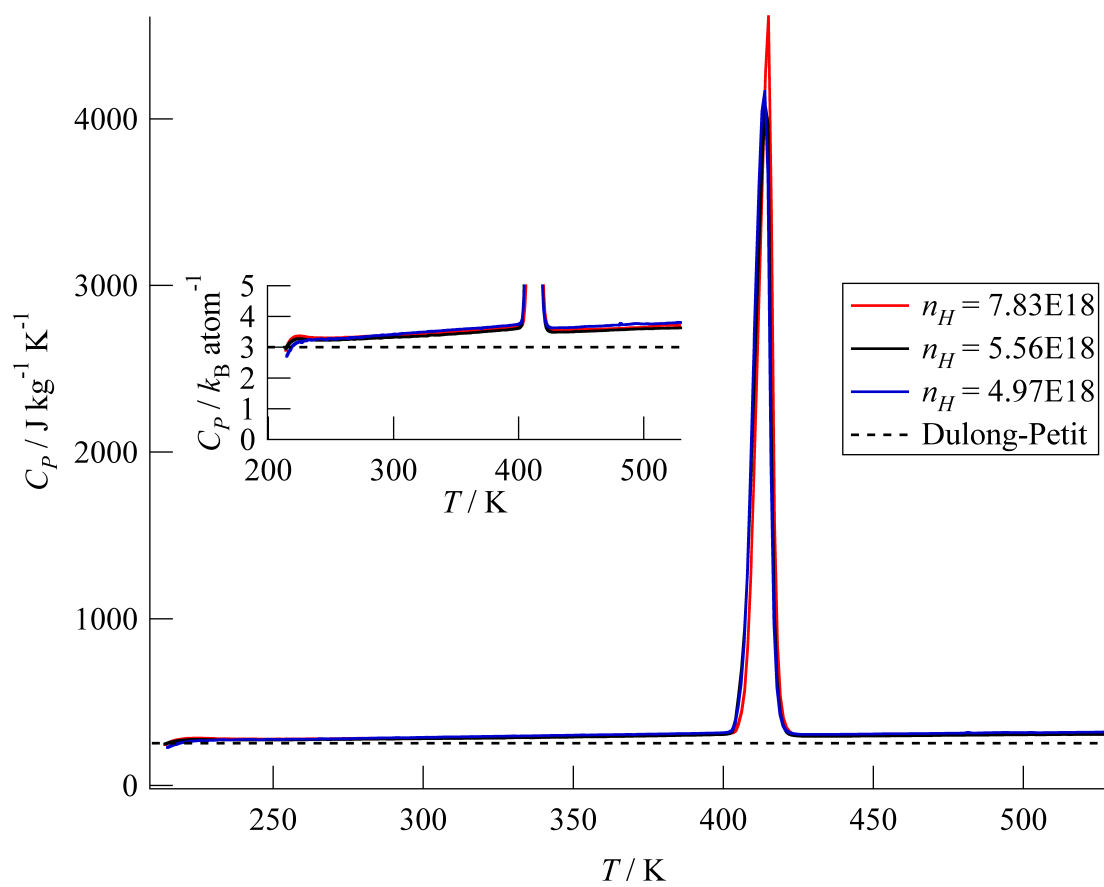


Figure S2: Heat capacity of ingot samples

2 Heating and Cooling Curves of Transport Properties

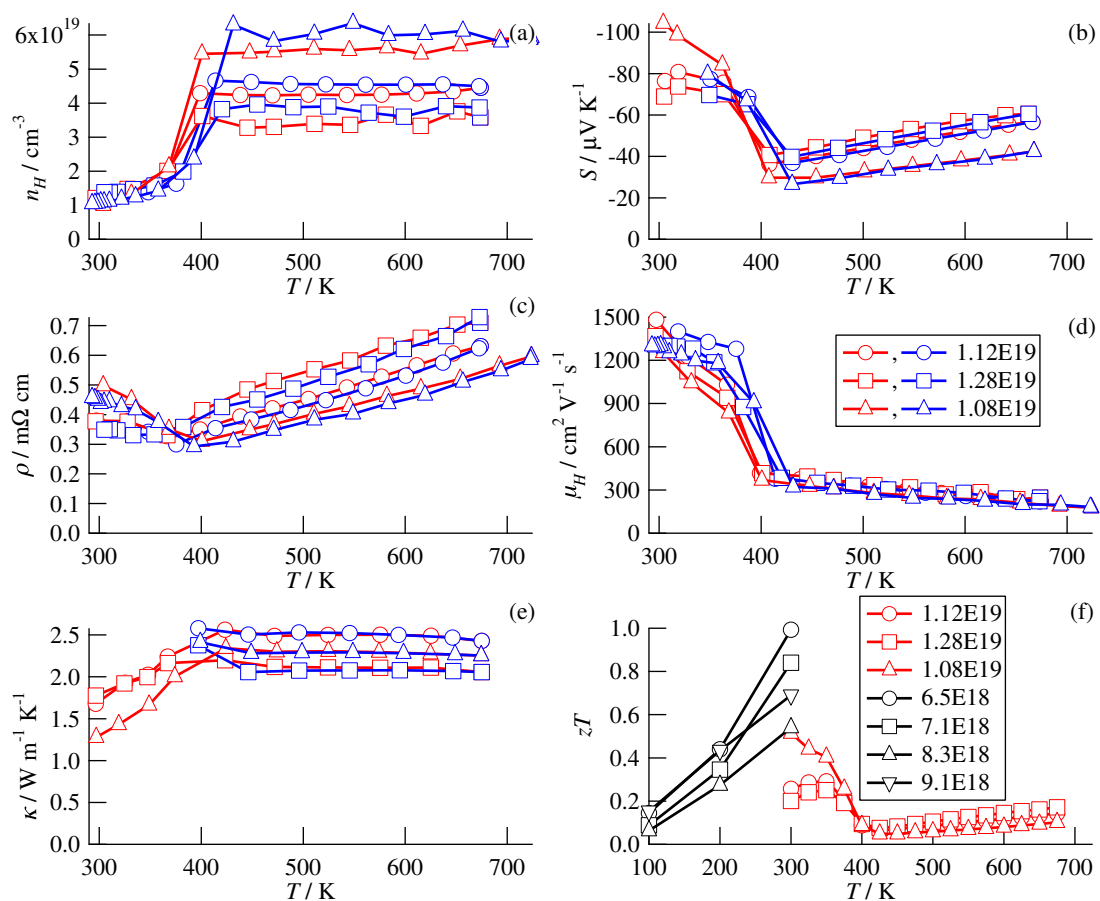


Figure S3: Transport properties of hot-pressed samples. Red curves are heating data, blue curves are cooling data. Black curves are from Aliev.^[1]

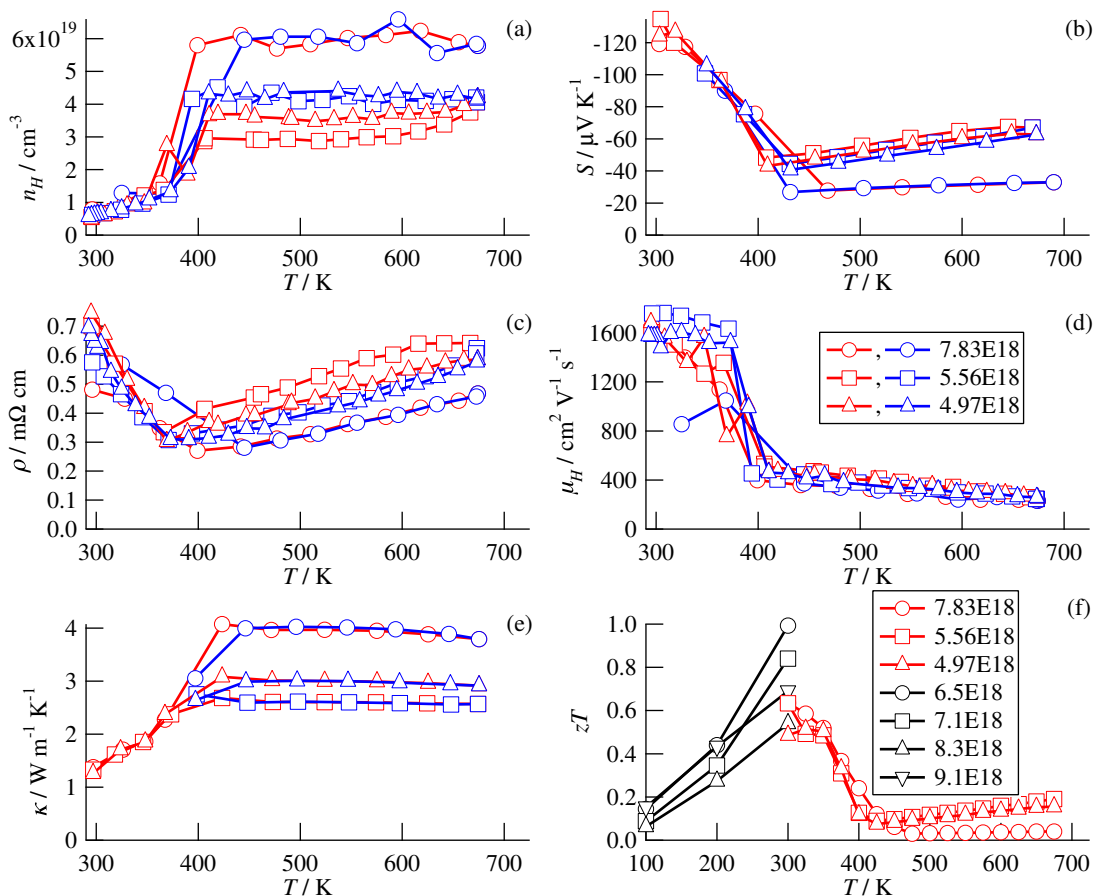


Figure S4: Transport properties of ingot samples. Red curves are heating data, blue curves are cooling data. Black curves are from Aliev.^[1]

3 Single Parabolic Band Model

The Hall carrier concentration n_H in a single parabolic band is given by Equation (1).^[2] m^* is the electron effective mass, k is Boltzmann's constant, T is absolute temperature, and h is Planck's constant. $F(j, \eta)$ is the Fermi integral of order j , given by Equation (2), where ϵ is the reduced electron energy, given by Equation (3). E is the electron energy. η is the reduced Fermi energy, given by Equation

(4). E_F is the Fermi energy in the material. The Hall factor r_H , which accounts for scattering and degeneracy effects, is given by Equation (5) when the electron mobility is limited by acoustic phonon scattering.^[2]

$$n_H = 4\pi \left(\frac{2m^*kT}{h^2} \right)^{3/2} F(1/2, \eta) \frac{1}{r_H} \quad (1)$$

$$F(j, \eta) = \int_0^\infty \frac{\epsilon^j d\epsilon}{1 + \exp(\epsilon - \eta)} \quad (2)$$

$$\epsilon = \frac{E}{kT} \quad (3)$$

$$\eta = \frac{E_F}{kT} \quad (4)$$

$$r_H = \frac{3}{4} F(-1/2, \eta) \frac{F(1/2, \eta)}{F(0, \eta)^2} \quad (5)$$

The Seebeck coefficient S of a single parabolic conduction band whose electron mobility is limited by acoustic phonon scattering is given by Equation (6), where e is the elementary charge.^[2]

$$S = -\frac{k}{e} \left(\frac{2F(1, \eta)}{F(0, \eta)} - \eta \right) \quad (6)$$

The resistivity ρ is given by Equation (7).

$$\rho = \frac{1}{n_H e \mu_H} \quad (7)$$

μ_H is the Hall mobility, which is given by Equation (8) for a single parabolic

band dominated by acoustic phonon scattering. μ_0 is a parameter that accounts for the material's density, speed of sound, and deformation potential, a quantity that describes how local lattice perturbations scatter electrons.^[3]

$$\mu_H = \mu_0 \frac{F(-1/2, \eta)}{2F(0, \eta)} \quad (8)$$

The thermal conductivity κ is given by Equation (9). κ is made up of two contributions, a lattice part κ_l and an electronic part κ_e . For a single parabolic band, κ_e is given by Equation (10). The Lorenz number L is given by Equation (11) when the electron mobility is limited by acoustic phonon scattering.^[2]

$$\kappa = \kappa_l + \kappa_e \quad (9)$$

$$\kappa_e = \frac{LT}{\rho} \quad (10)$$

$$L = \left(\frac{k}{e}\right)^2 \frac{3F(0, \eta)F(2, \eta) - 4F(1, \eta)^2}{F(0, \eta)^2} \quad (11)$$

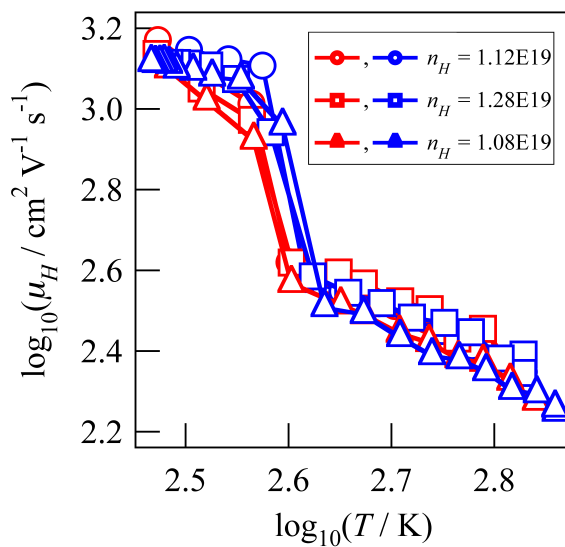
zT was calculated using Equations (12), (13), and (14). m_e is the electron rest mass. β depends only on the material properties and temperature, while S , L , and ψ are functions of η only.

$$zT = \frac{S^2}{L + (\psi\beta)^{-1}} \quad (12)$$

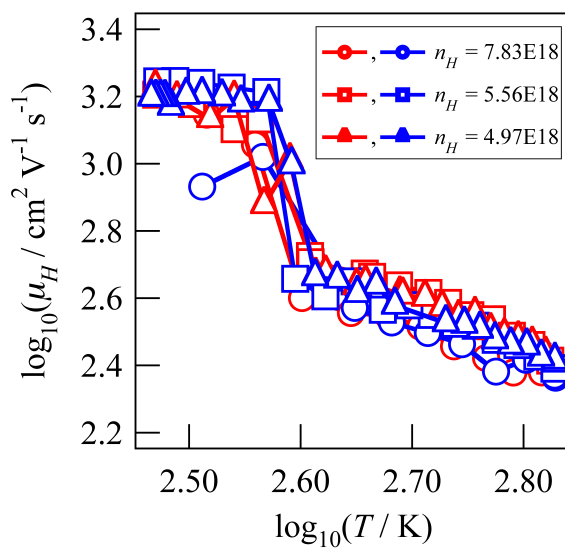
$$\psi = \frac{8\pi e}{3} \left(\frac{2m_e k}{h^2}\right)^{3/2} F(0, \eta) \quad (13)$$

$$\beta = \frac{\mu_0(m^*/m_e)^{3/2}T^{5/2}}{\kappa_l} \quad (14)$$

4 Scattering Mechanism



(a) Hot-Pressed



(b) Ingot

Figure S5: The slopes of log-log plots of Hall mobility versus temperature indicate the dominant scattering mechanism. Red curves are heating data, blue curves are cooling data.

The absolute values of the slopes of the curves in Figure S5 are all greater than 0.5, indicating that acoustic phonon scattering is the dominant scattering mechanism in this material at and above room temperature.^[2]

5 Seebeck Measurement Stability

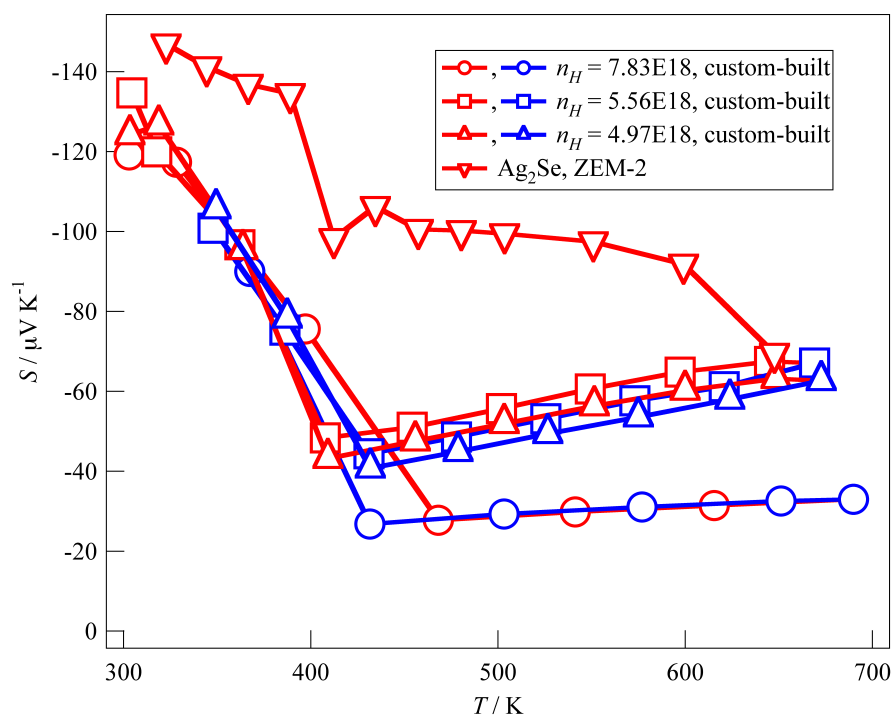


Figure S6: Seebeck coefficient of disks sliced from ingots. Red curves are heating data, blue curves are cooling data.

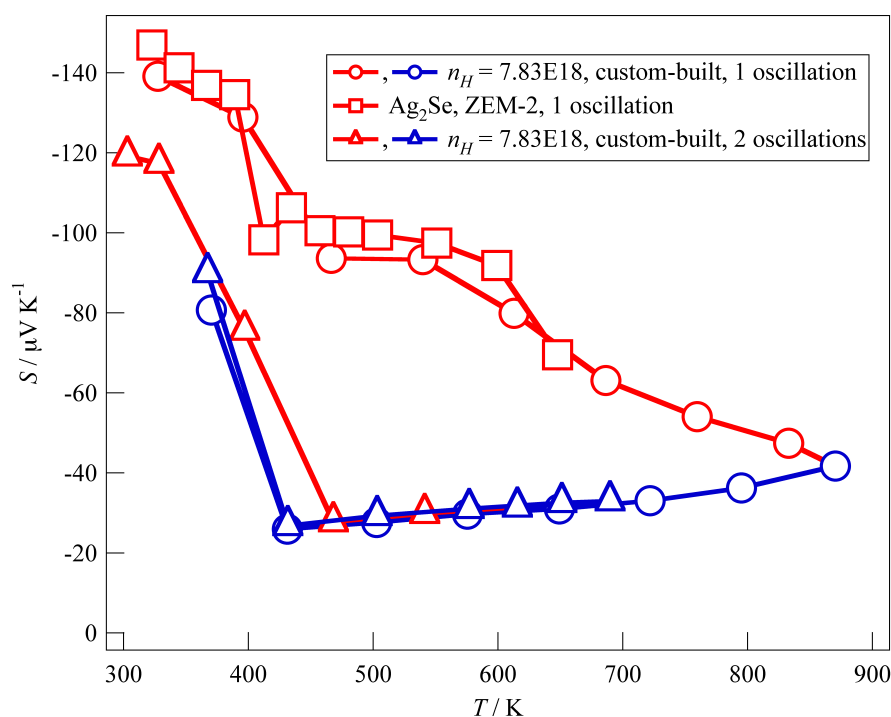


Figure S7: Effects of including an additional oscillation during measurement of the Seebeck coefficient of ingot samples of Ag_2Se . Red curves are heating data, blue curves are cooling data.

The Seebeck coefficients of the ingot samples are shown in Figure S6. The Seebeck coefficient of the Ag_2Se sample measured on the ZEM-2 shows a different temperature dependence than do the ingot samples measured on the custom-built apparatus. This could be caused by the different methods used to measure the Seebeck coefficient. The custom-built device was programmed to oscillate two times about each specified average temperature in order to allow any effects due to ramping of the average temperature to decay. The ZEM-2 was not programmed to do this. When an Ag_2Se ingot slice was measured in the custom-built device using only one oscillation, the Seebeck versus temperature curve shown in Figure S7 was obtained. This curve is plotted along with the Seebeck curve measured on the

ZEM-2 and the Seebeck curve measured with two oscillations on the custom-built device. The Seebeck curve measured on the ZEM-2 and the heating curve measured on the custom-built device are close to one another, suggesting that they are of similar composition and that unsteady heating effects can cause Ag_{2+x}Se to appear to have a high Seebeck coefficient.

6 XRD

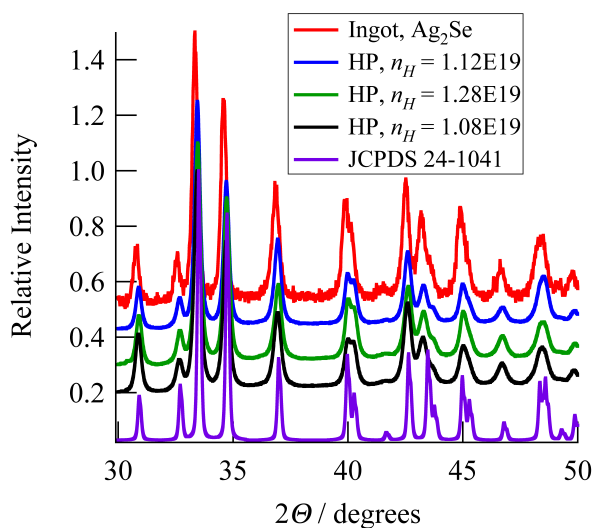


Figure S8: XRD scans of Ag_{2+x}Se at room temperature

References

- [1] F. Aliev, M. Jafarov, and V. Eminova. Thermoelectric Figure of Merit of Ag_2Se with Ag and Se Excess. *Atomic Structure and Nonelectronic Properties of Semiconductors*, 43(8):1013--1015, 2009.
- [2] V. I. Fistul. *Heavily Doped Semiconductors*. Plenum Press, 1969.
- [3] A. H. Wilson. *The Theory of Metals*. The Syndics of the Cambridge University Press, 1958.